Non-Uniform Sub-Nyquist Optical Sampling by Acousto-Optic Delay Modulation

Ross T. Schermer, *Member, IEEE, Member, OSA*, and Jason D. McKinney, *Senior Member, IEEE, Member, OSA*

(Invited Paper)

***Abstract*—This paper presents an optical sampler based on the combination of a mode-locked laser and external acousto-optic delay modulator, and demonstrates its use in a non-uniformly sub-sampled photonic link. Delay modulation of the laser's uniformly spaced pulse sequence produces a non-uniformly spaced optical pulse train, which subsequently sub-samples the microwave input of the photonic link. Using this non-uniform sub-sampler, microwave frequencies spanning a range exceeding 200 Nyquist zones are aliased to a single zone, with modulation sidebands added that uniquely identify the input frequency. This enables wideband spectral folding and frequency disambiguation, using a single sampler that is based on a high-stability pulsed laser.**

***Index Terms*—Frequency conversion, frequency estimation, microwave photonics, optoelectronic and photonic sensors, sampling methods, signal detection, spectroscopy.**

I. Introduction

THE scaling of analog-to-digital conversion techniques to wide frequency bandwidths (e.g., greater than 10 GHz) is complicated by the limited bandwidth of high-resolution electronic digitizers. Serial processing [1], which monitors regions of the spectrum sequentially in time using only a single digitizer, is unable to provide real-time monitoring of the processed bandwidth. Parallel processing [2], which separates the frequency spectrum into discrete channels, requires a large number of digitizers as the processed bandwidth increases. An alternative approach, capable of providing extremely wide instantaneous bandwidth using only a single digitizer, is to pre-process the wideband input prior to digitization via a sub-Nyquist sampling, or sub-sampling [3]–[5]. By sampling at a frequency f_s that is less than the Nyquist rate [6], input frequencies alias to a narrower intermediate frequency (IF) range, which has bandwidth equal to half the sampling frequency. This spectral folding process is depicted in Fig. 1. By proper choice of the sampling frequency, a wideband input can be converted to a narrowband output, and subsequently processed by few as a single electronic digitizer.

Manuscript received February 12, 2018; revised May 8, 2018; accepted May 22, 2018. Date of publication June 21, 2018; date of current version October 19, 2018. This work was supported by the U.S. Naval Research Laboratory. *(Corresponding author: Ross T. Schermer.)*

The authors are with the Optical Sciences Division, U.S. Naval Research Laboratory, Washington, DC 20375 USA (e-mail: ross.schermer@nrl.navy.mil; jason.mckinney@nrl.navy.mil).

Color versions of one or more of the figures in this paper are available online at http://ieeexplore.ieee.org.

Digital Object Identifier 10.1109/JLT.2018.2843288

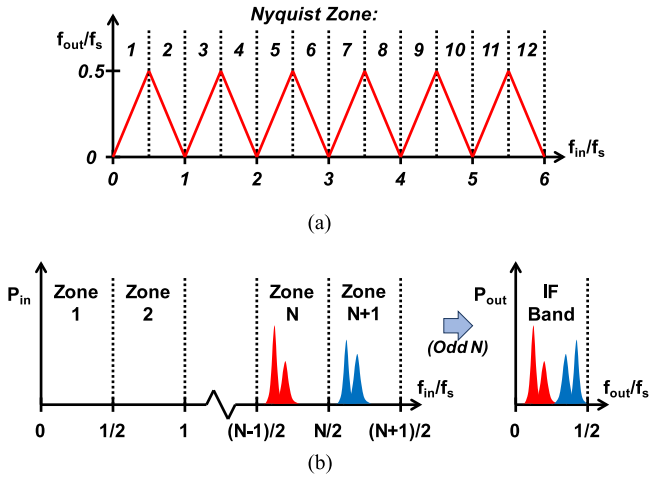

Fig. 1. Relationship between sub-sampler input frequency f_{in} and output frequency f_{out} (a), and spectral folding principle, in which input signals alias to an intermediate frequency (IF) band upon sub-sampling. Nyquist zones are labeled as indicated. P_{in} and P_{out} represent input and output power, respectively.

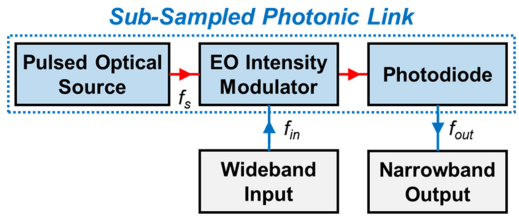

Fig. 2. Schematic diagram of a sub-sampled photonic link. Input frequencies f_{in} alias to output frequencies f_{out}.

Photonic links are particularly well suited to sub-sampling wideband signals, due to their low dispersion [7], [8], low frequency dependent loss [7], [8], and the availability of wide-bandwidth optical pulse sources. Sub-sampled photonic links have been realized in various forms [9]–[18], which generally include a pulsed optical source (i.e., optical sampler), electro-optic (EO) modulator, and photodiode, as shown in Fig. 2. In operation, a wideband signal input to the EO modulator is sub-sampled by the pulsed optical source, and the resulting narrowband IF signal is detected and output by the photodiode. A low-pass filter placed after the link can be used to suppress output frequencies greater than $f_s/2$, if necessary. Figures of merit for sub-sampled photonic links, including link gain, noise

figure, and output intercept points, have been demonstrated experimentally and theoretically [11], [12], [14].

For sub-sampling to be most useful, it is necessary to overcome the frequency ambiguity introduced by aliasing. Since sub-sampling causes multiple input frequencies to alias to the same output frequency, the input frequency (and thus the input spectrum) cannot be reconstructed by frequency measurement alone. For this reason, frequency disambiguation techniques have been developed, which typically involve the use of multiple samplers [18]–[22] (e.g., periodic samplers interleaved in time or operating at different frequencies), or a single sampler operating at a non-uniform sampling rate [17], [23], [24]. The non-uniform sampling approach requires only a single sampler, which from the optical perspective offers potential advantages in terms of size, weight, power and cost. However, a complication of non-uniform optical sub-sampling is that high-stability, pulsed laser sources inherently pulse at a uniform rate. Non-uniform sampling via pulsed laser therefore requires the modification of inter-pulse timing, in order to produce a sequence of non-uniformly spaced optical pulses.

This paper presents a non-uniform optical sampler that is based on the combination of a high-stability pulsed laser and an external acousto-optic delay modulator (AODM), and demonstrates its use in a non-uniformly sub-sampled photonic link. Section II introduces the non-uniform sampler, and Section III follows with measurements of sub-sampled link throughput. The latter includes a discussion of indicators present in the link output used to disambiguate the input frequency. Section IV discusses limits of frequency disambiguation using these indicators, and compares measurements with theory to demonstrate frequency disambiguation over a range exceeding 200 Nyquist zones. Section V discusses results in terms of sampling rates that are better matched to high-resolution digitizers. Section VI discusses frequency disambiguation of more complex signals, and Section VII concludes with a summary of results.

II. Non-Uniform Optical Sampler

The importance of the optical source to performance of a sub-sampled photonic link is illustrated in Fig. 3, which plots the normalized link gain of photonic links employing different optical sources. Other than the optical source, the composition of conventional and sub-sampled links denoted by the same link number (i.e., link 1 or link 2) was identical. Links 1 and 2 had photodiode bandwidths 32 GHz and 47 GHz, respectively. For sub-sampled links, gain denotes RF-to-IF conversion gain (i.e., ratio of IF signal power to RF input power), measured at output frequencies falling within the IF range $0-f_s/2$. In the case of an electro-optic (EO) frequency comb source (6 ps pulse width, 225 GHz rms bandwidth, 5 GHz repetition frequency) which was capable of non-uniform sampling, the frequency response was significantly degraded compared to the conventional phonic link employing a continuous-wave (CW) laser [17]. However, with a mode-locked laser source (0.3 ps pulse width, 1.573 THz bandwidth, 50.477 MHz repetition frequency) the frequency response was nearly identical to that of the conventional link. This is because the Fourier transform of the source intensity (i.e., its spectral field autocorrelation) weights the frequency response of a sub-sampled photonic link [17], [18] (as discussed in detail in the Appendix). In the case of the electro-optically generated frequency comb, the Fourier transform of the source intensity rolled off with frequency due to non-ideal pulse compression [17], giving rise to the modulation response in Fig. 3. In contrast, with the MLL the Fourier transform of the source intensity was sufficiently flat to process signals exceeding 40 GHz without degradation. The MLL, however, was not able to pulse at a non-uniform rate.

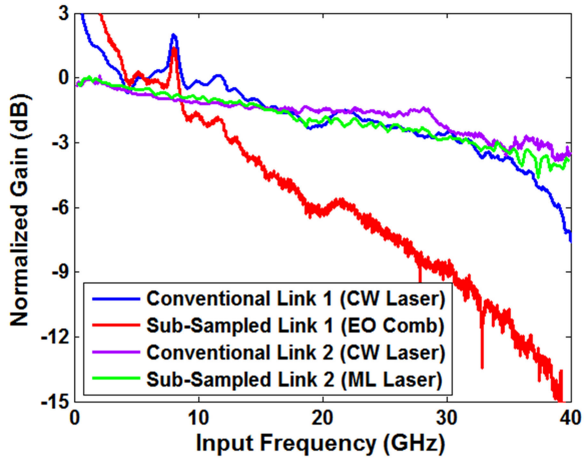

Fig. 3. Frequency response of photonic links employing different optical sources. Other than the optical source, composition of conventional link 1 and sub-sampled link 1 was identical. The same was true of conventional link 2 and sub-sampled link 2. With the EO comb source, sub-sampled link bandwidth was substantially degraded compared to the corresponding conventional link with CW laser source. In contrast, with the MLL source, sub-sampled link frequency response closely resembled that of the corresponding conventional link.

A schematic diagram of the non-uniform optical sampler presented in this work is displayed in Fig. 4(a), outlined in red. The sampler consists of a passively mode-locked laser and an external acousto-optic delay modulator. Although AODM operation is described elsewhere [25], a schematic diagram of the device is provided for reference in Fig. 4(b). In operation, the uniformly spaced pulse output of the MLL passes through the AODM, and the transit time (i.e., delay) of the AODM is modulated in order to produce a non-uniformly spaced pulse sequence.

The non-uniform sampler was realized using a MLL with 1554 nm center wavelength, 50.477 MHz pulse repetition frequency, and 1.573 THz (FWHM) optical bandwidth. As pulses from the laser passed through the AODM, the diffraction grating of the AODM acted as a spatial filter, reducing the optical bandwidth of the sampler to 145 GHz (measured with an optical spectrum analyzer). This bandwidth was sufficient to enable sub-sampling over a frequency range limited by other components of the photonic link, as discussed in Section III. However, spectral filtering by the AODM also added approximately 10 dB of optical loss, which in principle could have been avoided by using either a lower-bandwidth laser or a higher-bandwidth AODM. The time-average power output of the non-uniform sampler was 90 μW.

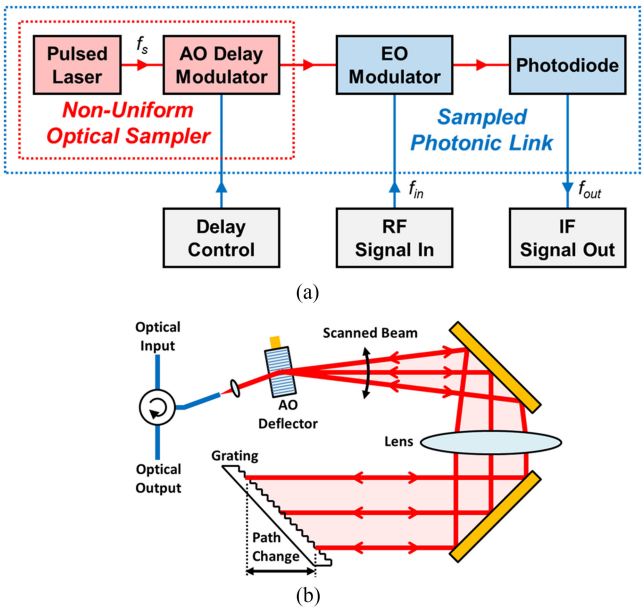

Fig. 4. Sub-sampled photonic link, with non-uniform optical sampler formed by combination of a pulsed laser and AODM (a), and schematic diagram of the AODM (b). Uniformly spaced laser pulses at repetition frequency f_S are converted to a non-uniformly-spaced optical pulse sequence by the AODM. Acousto-optic beam scanning in the AODM produces the necessary delay modulation. Pulses from the non-uniform sampler are passed through the EO modulator, sample its microwave input, and are detected by the photodiode.

Non-uniform sampling was accomplished by modulating the delay of the AODM according to the expression

$$\Delta\tau = \tau_{01}\sin\left(2\pi f_{M1}t\right) + \tau_{02}\,saw\left(f_{M2}t\right) \tag{1}$$

where t represents time, τ_{01} and τ_{02} are the delay modulation (DM) amplitudes at modulation frequencies f_{M1} and f_{M2}, respectively, and

$$saw\left(x\right) = x - floor\left(x + \frac{1}{2}\right) \tag{2}$$

is the sawtooth waveform. Delay was controlled using an arbitrary waveform generator, which applied a frequency-modulated (FM) voltage signal to the acousto-optic cell of the AODM. The conversion efficiency of the AODM (control frequency to time delay) was 394 fs/MHz. Thus, 8 MHz frequency deviation FM control signals used in this work implied delay modulation with 3.15 ps amplitude. This amplitude corresponded to 1.59×10^{-4} the repetition period of the MLL. DM therefore represented only a small perturbation of the sampling rate.

III. Non-Uniformly Sub-Sampled Photonic Link

The non-uniform sampler described in Section II served as optical source for the sub-sampled photonic link depicted in Fig. 4(a). The photonic link employed an EO Mach-Zehnder intensity modulator and PIN photodiode with 35 GHz and 47 GHz bandwidths, respectively. Voltage signals input to the EO modulator were optically sub-sampled, transmitted through 2 meters of single-mode optical fiber, and converted to voltage outputs by the photodiode. The time-average photocurrent was 15 μA, which was less than typical for photonic link [8], but minimized the potential influence of photodiode nonlinearity in the measurements.

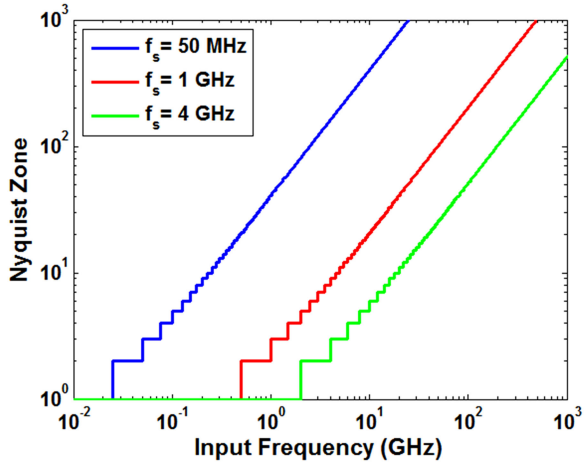

Fig. 5. Nyquist zone as a function of input frequency, at various uniform sampling frequencies. The blue curve corresponds to the 50.477 MHz laser repetition frequency used in this work. Red and green curves correspond to repetition frequencies better matched to high-resolution electronic digitizers.

The mapping of input frequency f_{in} to output frequency f_{out} due to aliasing is described in the case of uniform sampling by the expression

$$f_{out} = \left| f_{in} - \frac{Mf_s}{2} \right| \tag{3}$$

where

$$M = 2 \cdot floor\left(\frac{N}{2}\right). \tag{4}$$

Here N represents the Nyquist zone associated with the input frequency, which is the integer that minimizes f_{out} in (3). This convention for Nyquist zone numbering, although consistent with many sources including ADC manufacturers [26]–[30], is not universal. In particular, it differs from some conventions used to describe sub-sampled photonic links [11], [12], [17], [18].

Since non-uniform sampling in this work amounted to modulation of the MLL pulse spacing, (3) and its associated Nyquist zone definitions remain valid with the caveat that f_{out} represents the output *carrier* frequency. The *uniform* sampling frequency f_s corresponds to the repetition frequency of the laser. Fig. 5 plots Nyquist zone N versus input frequency for three laser repetition frequencies, including the 50.477 MHz laser repetition frequency used in this work. The other two are discussed in Section V.

Each discrete input frequency between 0–40 GHz predicted by (3) to produce the same 6.25 MHz output was launched sequentially into the sub-sampled photonic link using an analog signal generator, while the link output was monitored using an electrical spectrum analyzer (ESA). The measured relationship between input and output frequency is plotted in Fig. 6. Each discrete input frequency aliased to the same output frequency, confirming that the selected inputs were ambiguous with respect to sub-sampling. The output frequency 6.25 MHz lied approx-

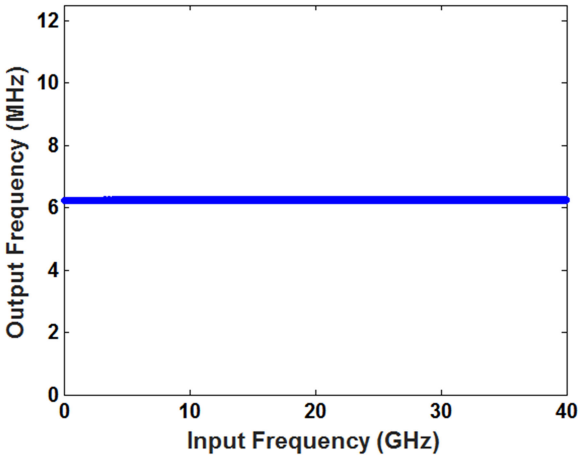

Fig. 6. Measured sub-sampled photonic link output frequency, for *discrete* input frequencies corresponding to the same 6.25 MHz output frequency in (3). Plotted points correspond to inputs within each of Nyquist zones 1–1584.

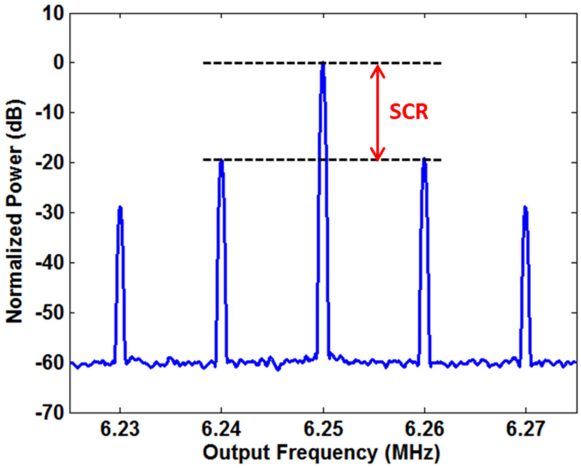

Fig. 7. Sub-sampled link output power spectrum, measured with inter-sample spacing modulated by a 10 kHz sinusoidal waveform. The input frequency was 10.10165 GHz, which aliased to a 6.25 MHz output carrier shown. Non-uniform sampling added modulation sidebands offset from the carrier by the 10 kHz modulation frequency. The sideband-to-carrier power ratio (SCR), shown, varied with the Nyquist zone pair.

imately halfway between the extremes (center and edge) of the IF band.

Although each selected input frequency aliased to the same output frequency, non-uniform sampling added modulation sidebands to the IF signal. The measured IF spectrum in Fig. 7 corresponds to sinusoidal delay modulation at 10 kHz ($\tau_{01} = 3.15\,\text{ps}$, $\tau_{02} = 0$, $f_{M1} = 10\,\text{kHz}$). With sinusoidal DM, the upper and lower modulation sidebands, offset from the carrier by $+f_{M1}$ and $-f_{M1}$, respectively, had equal power. More importantly, the sideband-to-carrier power ratio (SCR) depicted in Fig. 7 varied with Nyquist zone, scaling approximately as $[floor(N/2)]^2$. The measured SCR therefore represents a coarse indicator of the Nyquist zone, able to distinguish pairs of Nyquist zones, but not Nyquist zone parity. This coarse indicator is analogous to that demonstrated previously by non-uniform sampling using an EO comb source [17].

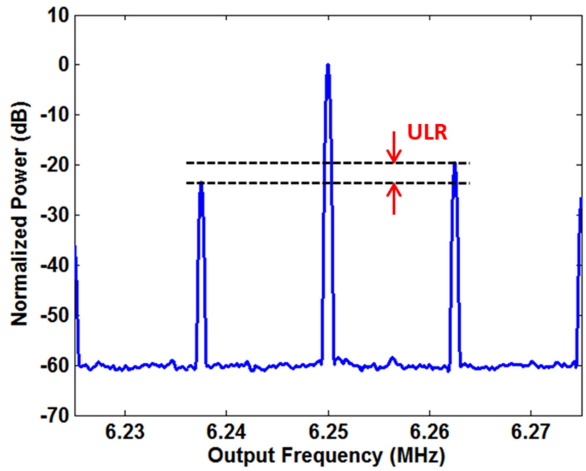

Fig. 8. Sub-sampled link output power spectrum, measured with inter-sample spacing modulated by a 12.5 kHz sawtooth waveform. The input frequency was 10.10165 GHz, which aliased to the 6.25 MHz output carrier shown. Non-uniform sampling added modulation sidebands offset from the carrier by the 12.5 kHz modulation frequency. The upper-to-lower sideband power ratio (ULR), shown, varied with Nyquist zone parity.

Non-uniform sampling with a sawtooth delay waveform produced a different result. The measured IF spectrum in Fig. 8 corresponds to sawtooth delay modulation at 12.5 kHz ($\tau_{02} = 3.15\,\text{ps}$, $\tau_{01} = 0$, $f_{M2} = 12.5\,\text{kHz}$). With sawtooth DM, the upper and lower modulation sidebands, offset from the carrier by $+f_{M2}$ and $-f_{M2}$, respectively, had unequal power. More importantly, the upper sideband-to-lower sideband power ratio (ULR) depicted in Fig. 8 varied with Nyquist zone parity (i.e., whether *N* was even or odd). The measured ULR therefore represents a fine indicator of the Nyquist zone, able to distinguish zone parity.

Together, the fine and coarse frequency indicators (SCR and ULR) provide sufficient information to disambiguate the input frequency of the sub-sampled photonic link. For this reason, sinusoidal and sawtooth DM waveforms were simultaneously applied to the AODM ($\tau_{01} = \tau_{02} = 3.15\,\text{ps}$, $f_{M1} = 10\,\text{kHz}$, $f_{M2} = 12.5\,\text{kHz}$), resulting in the IF spectrum in Fig. 9. The SCR was measured at 10 kHz offset from the carrier, and the ULR at 12.5 kHz offset, as shown. Fig. 10 and Fig. 11 plot measured SCR and ULR for each discrete input frequency from 0–40 GHz that aliased to the same 6.25 MHz output. These figures are similar to those reported by the authors in [31], with the exception that the dynamic range in Fig. 10 has been improved by approximately 10 dB. In Fig. 10, the SCR varies discretely with incremental steps of two Nyquist zones. In Fig. 11, the ULR depends strongly on Nyquist zone parity, with ULRs of adjacent Nyquist zones approximately the inverse of each other. Both trends are demonstrated over more than 2.5 decades in frequency.

The solid line in Fig. 10 represents a least squares fit of the measured SCR to the theoretical expression [25]

$$SCR_{(CL)} = \left[\frac{J_1\left(2\pi f_{in}\tau_{01}\right)}{J_0\left(2\pi f_{in}\tau_{01}\right)}\right]^2 \tag{5}$$

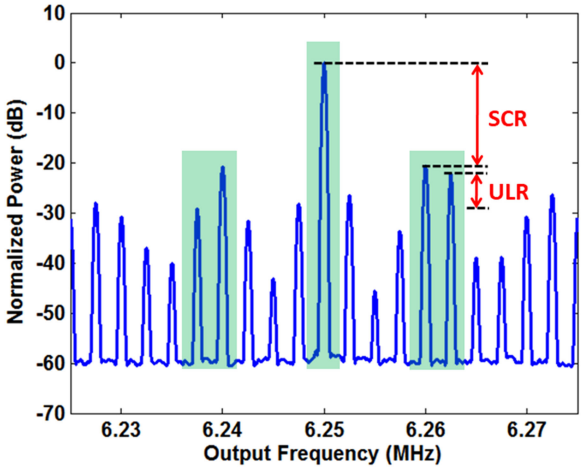

Fig. 9. Sub-sampled link output power spectrum, measured with inter-sample spacing rate modulated by 10 kHz sinusoidal and 12.5 kHz sawtooth waveforms. The input frequency was 10.10165 GHz. Sidebands offset 10 kHz from the 6.25 MHz output carrier correspond to sinusoidal modulation, and have equal magnitude. Sidebands offset 12.5 kHz from the carrier correspond to sawtooth modulation, and have different magnitude. Other sidebands are the result of harmonic and intermodulation distortions. SCR and ULR varied with Nyquist zone pair and Nyquist zone parity, respectively.

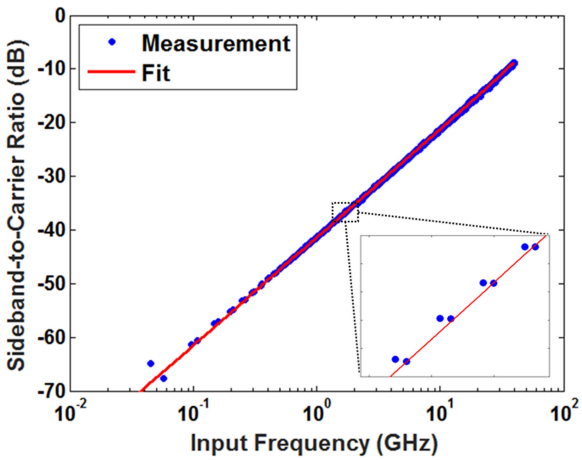

Fig. 10. Measured SCR (blue points), and least squares fit of data to (5) (red curve). The measured SCR tracks (5) in discrete increments of two Nyquist zones. Measured SCR is thus a coarse indicator of Nyquist zone and input frequency.

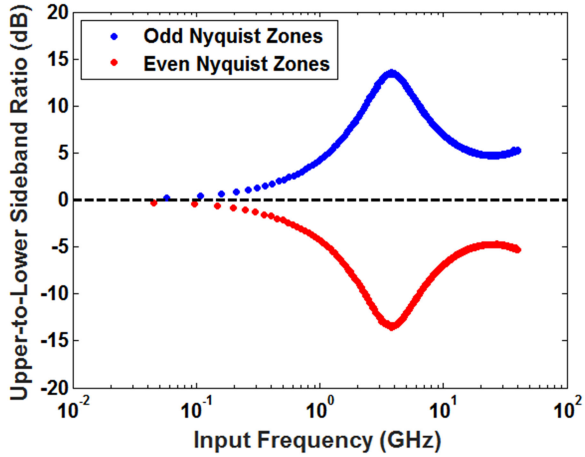

Fig. 11. Measured ULR corresponding to odd Nyquist zones (blue points) and even Nyquist zones (red points). The ULR is greater than 0 dB for odd zones, and less than 0 dB for even zones. Measured ULR is thus a fine indicator of Nyquist zone and input frequency.

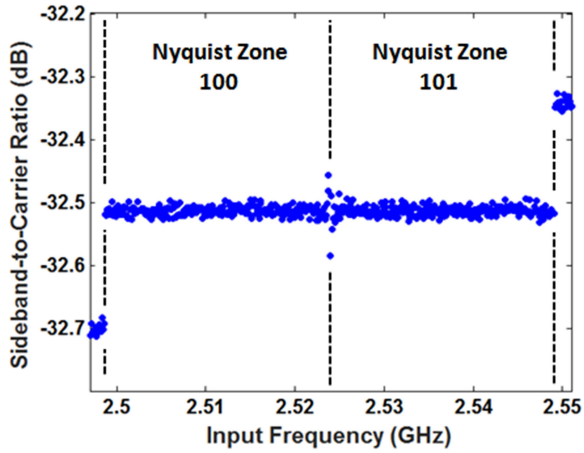

Fig. 12. Measured SCR for input frequencies spanning two adjacent Nyquist zones (zones 100 and 101). SCR did not vary significantly with input frequency within each Nyquist zone.

corresponding to the SCR of a *conventional* photonic link experiencing sinusoidal delay modulation. In (5), τ_{01} represents the DM amplitude, and J_m is a Bessel function of order m. The least squares fit of measured SCR to (5) yielded a best fit delay amplitude of 2.72 ps. This was 14% lower than predicted in Section II from the (frequency-to-delay) conversion efficiency of the AODM, and likely due to the variations in the device's acoustic frequency response.

Although a theoretical treatment of the ULR is beyond the scope of this paper, the unequal sidebands in Fig. 8 can be regarded as the combination of dual sideband (DSB) and single-sideband (SSB) modulation. SSB modulation can involve the phased superposition of two (or more) fields, modulated by signals that are 90° out of phase with respect to one another [32]. Propagation through the AODM entails two acousto-optic (AO) beam deflections, one on each pass though the AO cell. It is possible that latency between these two AO interactions contributed to the partial SSB modulation depicted in Fig. 8.

Fig. 12 plots measured SCR for input frequencies spanning the 100th and 101st Nyquist zone, which illustrates that the SCR was independent of input frequency within each Nyquist zone. The measured ULR was also independent of input frequency within each zone.

The measured frequency response of the non-uniformly sub-sampled photonic link is shown in Fig. 13, which plots normalized RF to IF conversion gain (measured at the IF carrier frequency) as a function of input frequency. For comparison, Fig. 13 also plots the link gain measured with delay modulation amplitude reduced to zero (i.e., uniform sub-sampling). This indicates that strong delay modulation caused the link gain to decrease, an effect attributable to the generation of delay modulation sidebands. Fig. 13 also plots the gain measured for a conventional link with CW laser source (but otherwise identical components). This indicates that for weak delay modulation,

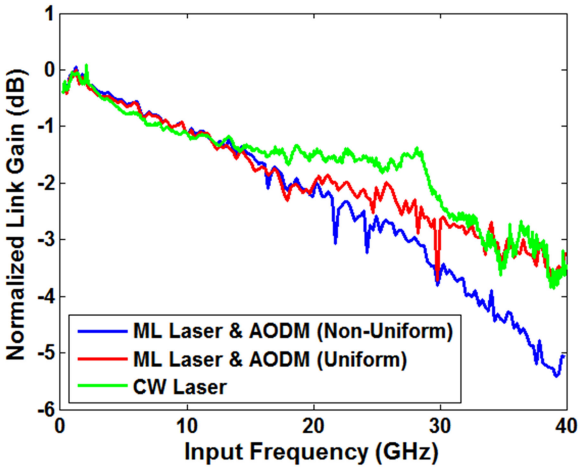

Fig. 13. Measured link gain of the non-uniformly sub-sampled photonic link with pulsed source composed of a MLL and AODM (blue curve). Normalized to its peak value. For comparison, link gain is also plotted for a uniformly sub-sampled photonic link with pulsed source composed of the same MLL and AODM, but without delay modulation applied (red curve). This indicates that strong delay modulation caused link gain to decrease, an effect attributable to the generation of delay modulation sidebands. The gain of a conventional link with CW laser source (but otherwise identical components) is also plotted (green curve). This indicates that the frequency response of the sub-sampled link with MLL and AODM closely approximated that of the conventional link, in the limit of weak delay modulation.

the frequency response of the sub-sampled link with MLL and AODM approximated that of the conventional link.

IV. Frequency Disambiguation

The input frequency indicators discussed in Section III (SCR and ULR) rely on measurements of spectral amplitude, and as such, measurement errors affect the ability to discriminate Nyquist zones using the SCR and ULR.

In the case of coarse frequency disambiguation, the theoretical SCR for all input frequencies associated with Nyquist zone *N* is given by

$$SCR = \left[\frac{J_1\left(M\pi f_s \tau_{01}\right)}{J_0\left(M\pi f_s \tau_{01}\right)}\right]^2. \tag{6}$$

This follows from application of (5) to delay modulation of a pulsed laser frequency spectrum (a pulsed laser resembles a CW laser modulated at integer multiples of the laser repletion frequency). For small arguments, the Bessel functions in (6) can be approximated [33] to yield

$$SCR \cong \left(M\pi f_s \tau_{01}/2\right)^2. \tag{7}$$

The relative difference between SCRs of adjacent Nyquist zone pairs, *SCR(N)* and *SCR(N ± 2)*, can thus be written as

$$\frac{|SCR\left(N\pm 2\right) - SCR\left(N\right)|}{SCR\left(N\right)} \cong \frac{4}{M}\left(1 \pm \frac{1}{M}\right) \quad (N \pm 1 > 2). \tag{8}$$

In order to discriminate Nyquist zone *N* from all other Nyquist zone pairs, the relative error of an SCR measurement must be less than half the smaller of $|[SCR(N \pm 2)/SCR(N)] - 1|$. The SCR relative error limit $\varepsilon_{SCR(\max)}$, beyond which coarse frequency disambiguation fails, is thus given by

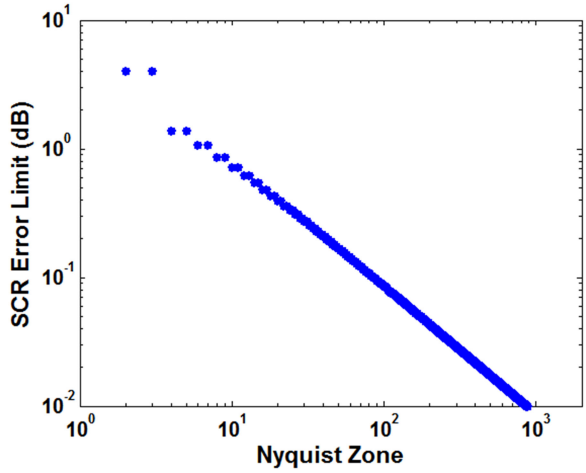

Fig. 14. SCR error limit, beyond which coarse frequency disambiguation fails. From (9). Error tolerance decreases as Nyquist zone increases.

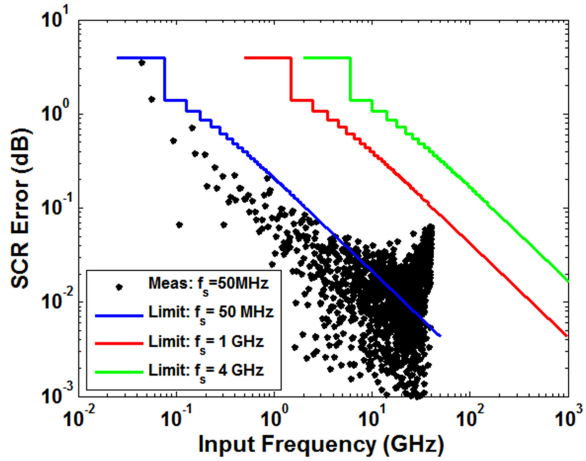

Fig. 15. SCR error (black points), measured at laser repetition frequency 50.477 MHz, and SCR error limits (solid curves) at sampling frequencies 50.477 MHz, 1 GHz and 4 GHz. SCR error is low enough to disambiguate input frequencies 0.25–5.274 GHz at the sampling frequency 50.477 MHz. This corresponds to Nyquist zones 2-209. With increasing sampling frequency, the error limit shifts to higher input frequency.

$$\varepsilon_{SCR(\max)} \cong \begin{cases} \frac{3}{2} & (1 < N \leq 3) \\ \frac{2}{M}\left(1 - \frac{1}{M}\right) & (3 < N) \end{cases}. \tag{9}$$

Fig. 14 plots the SCR relative error limit as a function of Nyquist zone. Error is expressed on a decibel scale via [34]

$$\varepsilon_{\mathrm{dB}} = 10\,\log_{10}\left(1+\varepsilon\right). \tag{10}$$

It is apparent from Fig. 14 that the tolerance for SCR error becomes more stringent as the Nyquist zone increases.

Fig. 15 plots the relative SCR measurement error ε_{SCR} as a function of input frequency. This was calculated by comparing measured and theoretical SCR values, SCR_{meas} and *SCR*, respectively, using the expression

$$\varepsilon_{SCR} = \frac{|SCR_{meas} - SCR|}{SCR}. \tag{11}$$

For comparison, the SCR error limit $\varepsilon_{SCR(\max)}$ is also plotted in Fig. 15. The SCR measurements were sufficiently accurate to allow coarse frequency disambiguation over the input frequency range 0.025–5.274 GHz, corresponding to Nyquist zones 2–209.

For fine frequency disambiguation, it is necessary to determine whether the ULR associated with Nyquist zone N (ULR_N) is greater than or less than one. The ULR relative error limit $\varepsilon_{ULR(\max)}$, beyond which fine frequency disambiguation fails, is therefore given by

$$\varepsilon_{ULR(\max)} = \frac{|ULR - 1|}{ULR}. \tag{12}$$

It is readily apparent from Fig. 11 that the error in all ULR measurements was low enough to enable fine frequency disambiguation over the range 0.025–40 GHz, corresponding to Nyquist zones 2–1584. As both coarse and fine frequency disambiguation were demonstrated across Nyquist zones 2–209, input frequencies in the range 0.050–5.274 GHz can be regarded as fully disambiguated.

The SCR measurement error in Fig. 15 followed a linear trend at low input frequency, giving way to a more scattered distribution at high frequency. Low frequency error was dominated by amplitude modulation (AM) within the AODM, which resulted in AM sidebands of the order -70 dBc. At lower input frequency, for which the DM sidebands were relatively weak, AM had a greater influence on the measured SCR and was thus a larger source of relative error. At higher input frequency, the SCR error was more widely scattered. Although this was clearly due to fluctuations in the measured SCR, the source these fluctuations, and methods to minimize them, have not been systematically tested.

V. Disambiguation at Higher Repetition Frequencies

The laser repetition frequency used in this work was dictated by laser availability rather than choice. The 50.477 MHz repetition frequency allowed SCR and ULR to be characterized over the wide range of 1584 Nyquist zones from 0–40 GHz, producing clear, quasi-continuous frequency dependencies as shown in Figs. 10 and 11. However, the resulting 25.239 MHz IF bandwidth is substantially lower than bandwidths of many high-resolution digitizers [35]–[38]. In order to provide a better match to high-resolution electronic digitizers with bandwidths of the order 1–4 GHz, uniform sampling frequencies of the order 1–4 GHz would be more appropriate (allowing for some oversampling by the digitizer). For this reason, Figs. 5 and 15 plot Nyquist zone and SCR error limit, respectively, at the uniform sampling frequencies 1 GHz and 4 GHz. Increasing the sampling rate causes both curves to shift proportionally with respect to the input frequency.

The theoretical SCR, on the other hand, varies with input frequency according to

$$SCR = \left[\frac{J_1\left(2\pi f_{in}\tau_{01}\right)}{J_0\left(2\pi f_{in}\tau_{01}\right)}\right]^2 \quad (f_{out} = 0). \tag{13}$$

This follows from combination of Eqs. (3), (4) and (6). Equation (13) implies that the theoretical SCR follows the same trend, depicted in red in Fig. 10, regardless of sampling frequency. The SCR error at higher sampling frequencies therefore depends on how well measured SCR matches this particular trend.

Although prediction of SCR error at higher laser repetition frequencies was not attempted, it is clear from Fig. 15 that if measured SCR error was similar to that shown (i.e., if error was independent of the laser), then higher repetition frequency would enable frequency disambiguation over a wider frequency range. The measured error plotted in Fig. 15 is below the disambiguation limit for laser repetition frequencies 1 GHz and 4 GHz, across the entire tested input range 0–40 GHz.

VI. Extension to Finite Bandwidth Signals

Having demonstrated frequency disambiguation for monochromatic input signals, the next step is to consider more complex inputs. Although a detailed discussion is beyond the scope of this paper, insight can be provided by limiting the consideration to signals confined to a single Nyquist zone. With this restriction, the sinusoidal DM embodied by (6) amounts to sinusoidal phase modulation (ΦM) with the amplitude

$$\varphi_0 = M\pi f_s \tau_0. \tag{14}$$

Coarse frequency disambiguation therefore involves determination of the phase modulation amplitude in (14). Methods for characterizing ΦM are well-established [39]–[43], and applicable to the modulation of complex carrier signals [44].

In the simple case of a signal with bandwidth sufficiently less than the modulation frequency f_M, SCR can be measured directly from the frequency spectrum, as in Section III. This motivates the use of high modulation frequency. The high-frequency limits of AO delay modulation, however, have not been fully explored. For wider bandwidth signals, combination of modulated and unmodulated signals (e.g., differential or interferometric measurement) may be more appropriate. For example, subtraction of modulated and unmodulated signals (i.e., carrier suppression) could allow the strength of the modulation sidebands to be measured, even for wide bandwidth signals. Comparison with the (independently measured) carrier would then yield the SCR. Regardless of the method, the agreement between measured and theoretical SCRs in Sections III and IV supports the validity of (14), over more than 2.5 decades in frequency. Implementation with specific systems, and performance under various scenarios, remain topics for future work.

VII. Conclusion

This paper introduces a method for externally modulating the inter-pulse timing of a pulsed laser, thereby producing a non-uniform optical sampler. Acousto-optic delay modulation provided continuous, picosecond-scale delay control. When used as the optical source for a sub-sampled photonic link, the non-uniform sampler allowed input frequencies spanning more than 200 Nyquist zones to be aliased to the width of a single Nyquist zone and uniquely identified. This approach enables wideband spectral folding and frequency disambiguation, using a single sampler that is based on a high-stability pulsed laser.

APPENDIX

The time-dependent optical intensity $P_{PD}(t)$ incident on the photodiode in Fig. 2 depends on the optical intensity of pulsed source $P_S(t)$ and the transmissivity of the EO modulator $T_{EOM}(t)$, according to the relation

$$P_{PD}(t) = P_S(t)\, T_{EOM}(t). \tag{15}$$

The Fourier transform of this expression with respect to time *t* is given by

$$\tilde{P}_{PD}(f) = \tilde{P}_S(f) \otimes \tilde{T}_{EOM}(f) \tag{16}$$

where $\otimes$ represents a convolution with respect to frequency *f*, and $T_{EOM}(f)$, $P_S(f)$ and $P_{PD}(f)$ represent Fourier transforms of the modulator transmissivity, source intensity and intensity at the photodiode, respectively. Neglecting photodiode distortions (i.e., in the low-power limit), the Fourier transform of the detected photocurrent can be written concisely as

$$\tilde{I}_{PD}(f) = \left[\tilde{P}_S(f) \otimes \tilde{T}_{EOM}(f)\right] \tilde{\Re}_{PD}(f) \tag{17}$$

where $\Re_{PD}(f)$ represents the photodiode responsivity. From (17) it is clear that the Fourier transform of the source intensity weights the frequency response of the sub-sampled photonic link. In particular, the bandwidth of the source intensity impacts the range of input frequencies that will alias to the first Nyquist zone.

It should be noted that the Fourier transform of intensity equals the frequency-domain autocorrelation of the field (by the Wiener-Khinchin theorem). It differs from the power spectral density, which is the squared magnitude of the field in the frequency-domain.

REFERENCES

[1] M. Da Silva, "Real-time spectrum analysis and time-correlated measurements applied to nonlinear system characterization," in *Modern RF and Microwave Measurement Techniques*, V. Teppati *et al.*, Eds. New York, NY, USA: Cambridge Univ. Press, 2013, pp. 64–97.

[2] G. W. Anderson, D. C. Webb, A. E. Spezio, and J. N. Lee, "Advanced channelization for RF, microwave, and millimeterwave applications," *Proc. IEEE*, vol. 79, no. 3, pp. 355–388, Mar. 1991.

[3] M. Mishali and Y. C. Eldar, "Sub-Nyquist sampling," *IEEE Signal Process. Mag.*, vol. 28, no. 6, pp. 98–124, Nov. 2011.

[4] M. Mishali and Y. C. Eldar, "From theory to practice: Sub-Nyquist sampling of sparse wideband analog signals," *IEEE J. Sel. Topics Signal Process.*, vol. 4, no. 2, pp. 375–391, Apr. 2010.

[5] R. Maleh, G. L. Fudge, F. A. Boyle, and P. E. Pace, "Analog-to-information and the Nyquist folding receiver," *IEEE J. Emerg. Sel. Topics Circuits Syst.*, vol. 2, no. 3, pp. 564–578, Sep. 2012.

[6] A. J. Jerri, "The shannon sampling theorem-its various extensions and applications: A tutorial review," *Proc. IEEE*, vol. 65, no. 11, pp. 1565–1596, Nov. 1977.

[7] C. H. Cox, "Frequency response of links," in *Analog Optical Links: Theory and Practice*. Cambridge, U.K.: Cambridge Univ. Press, 2006, pp. 91–158.

[8] V. J. Urick *et al.*, "Propagation effects," in *Fundamentals of Microwave Photonics.* Hoboken, NJ, USA: Wiley, 2015, pp. 166–204.

[9] P. W. Juodawlkis, J. J. Hargreaves, R. D. Younger, G. W. Titi, and J. C. Twichell, "Optical down-sampling of wide-band microwave signals," *J. Lightw. Technol.*, vol. 21, no. 12, pp. 3116–3124, Dec. 2003.

[10] J. Kim *et al.*, "Photonic subsampling analog-to-digital conversion of microwave signals at 40-GHz with higher than 7-ENOB resolution," *Opt. Express*, vol. 16, pp. 16509–16515, Oct. 2008.

[11] J. D. McKinney and K. J. Williams, "Sampled analog optical links," *IEEE Trans. Microw. Theory Techn.*, vol. 57, no. 8, pp. 2093–2099, Aug. 2009.

[12] J. D. McKinney and V. J. Urick, "Radio-frequency down-conversion via sampled analog optical links," U.S. Naval Res. Lab., Washington, DC, USA, Rep. NRL/MR/5650-10-9275, 2010.

[13] J. D. McKinney, V. J. Urick, and J. Briguglio, "Optical comb sources for high dynamic-range single-span long-haul analog optical links," *IEEE Trans. Microw. Theory Techn.*, vol. 59, no. 12, pp. 3249–3257, Dec. 2011.

[14] B. C. Pile and G. W. Taylor, "Performance of subsampled analog optical links," *J. Lightw. Technol.*, vol. 30, no. 9, pp. 1299–1305, May 2012.

[15] T. P. McKenna *et al.*, "Wideband photonic compressive sampling analog-to-digital converter for RF spectrum estimation," in *Proc. Opt. Fiber Commun. Conf.*, Anaheim, CA, USA, 2013, pp. 1–3.

[16] P. Ghelfi *et al.*, "A fully photonics-based coherent radar system," *Nature* vol. 507, pp. 341–345, Mar. 2014.

[17] S. R. Harmon and J. D. McKinney, "Broadband RF disambiguation in subsampled analog optical links via intentionally-introduced sampling jitter," *Opt. Express*, vol. 22, pp. 23928–23937, Oct. 2014.

[18] S. R. Harmon and J. D. McKinney, "Precision broadband RF signal recovery in subsampled analog optical links," *IEEE Photon. Technol. Lett.*, vol. 27, no. 6, pp. 620–623, Mar. 2015.

[19] W. Black and D. Hodges, "Time interleaved converter arrays," in *Proc. IEEE Int. Solid-State Circuits Conf. Dig. Tech. Papers*, Feb. 1980, vol. XXIII, pp. 14–15.

[20] R. Venkataramani and Y. Bresler, "Perfect reconstruction formulas and bounds on aliasing error in sub-Nyquist nonuniform sampling of multiband signals," *IEEE Trans. Inf. Theory*, vol. 46, no. 6, pp. 2173–2183, Sep. 2000.

[21] C. Vogel and H. Johansson, "Time-interleaved analog-to-digital converters: Status and future directions," in *Proc. Int. Symp. Circuits Syst.*, 2006, no. 4, pp. 3386–3389.

[22] I. Coddington *et al.*, "Dual-comb spectroscopy," *Optica*, vol. 3, pp. 414–426, Apr. 2016.

[23] A. Aldroubi and K. Gröchenig, "Nonuniform sampling and reconstruction in shift-invariant space," *SIAM Rev.*, vol. 43, pp. 585–620, 2001.

[24] J. A. Tropp, J. N. Laska, M. F. Duarte, J. K. Romberg, and R. G. Baraniuk, "Beyond Nyquist: Efficient sampling of sparse bandlimited signals," *IEEE Trans. Inf. Theory*, vol. 56, no. 1, pp. 520–544, Jan. 2010.

[25] R. T. Schermer *et al.*, "Acousto-optic delay modulation of a photonic signal," in *Proc. Conf. Lasers Electro-Opt.*, San Jose, CA, USA, 2016, pp. 1–2.

[26] "Fundamentals of sampled data systems," in *The Data Conversion Handbook*, W. Kester, Ed. Oxford, U.K.: Newnes, 2005, pp. 57–146.

[27] "Folded frequency calculator," Maxim Integrated, San Jose, CA, USA, Appl. Note 3716, Dec. 2005. [Online]. Available: https://pdfserv.maximintegrated.com/en/an/AN3716.pdf

[28] P. Poshala, "Why oversample when undersampling can do the job?" Texas Instrum., Dallas, TX, USA, Appl. Rep. SLAA594A, Jul. 2013. [Online]. Available: http://www.ti.com/lit/an/slaa594a/slaa594a.pdf

[29] "High speed DACs," Tektronix, Beaverton, OR, USA, App. Note, Jul. 2014. [Online]. Available: https://www.tek.com/document/application-note/high-speed-dacs

[30] S. W. Ellingson, "Receivers," in *Radio Systems Engineering*. Cambridge, U.K.: Cambridge Univ. Press, 2016, pp. 446–485.

[31] R. T. Schermer and J. D. McKinney, "Disambiguation of sub-sampled photonic links by acousto-optic delay modulation," in *Proc. IEEE Avionics Veh. Fiber-Opt. Photon. Conf.*, New Orleans, LA, USA, 2017, pp. 35–36.

[32] S. L. Dawson, "Exciter and transceiver design," in *Single-Sideband Systems and Circuits*, W. E. Sabin and E. O. Schoenike, Eds. New York, NY, USA: McGraw-Hill, 1987, pp. 135–180.

[33] G. B. Arfken and H. J Weber, "Bessel functions," in *Mathematical Methods for Physicists*, 4th ed. New York, NY, USA: Academic, 1995, pp. 627–692.

[34] G. Taraldsena *et al.*, "Uncertainty of decibel levels," *J. Acoust. Soc. Amer.*, vol. 138, pp. EL264–EL269, Sep. 2015.

[35] R. Walden, "Analog-to-digital converter survey and analysis," *IEEE J. Sel. Areas Commun.*, vol. 17, no. 4, pp. 539–550, Apr. 1999.

[36] K. G. Merkel and A. L. Wilson, "A survey of high performance analog-to-digital converters for defense space applications," in *Proc. IEEE Aerospace Conf.*, Big Sky, MT, USA, Mar. 2003, vol. 5, pp. 2415–2427.

[37] B. Le *et al.*, "Analog-to-digital converters [A review of the past, present, and future]," *IEEE Signal Process. Mag.*, vol. 22, no. 6, pp. 69–77, Nov. 2005.

[38] B. Murmann, "ADC performance survey 1997–2017," [Online]. Available: http://www.stanford.edu/∼murmann/adcsurvey.html

[39] W. M. Waters and B. R. Jarrett, "Bandpass signal sampling and coherent detection," *IEEE Trans. Aerosp. Electron. Syst.*, vol. AES-18, no. 6, pp. 731–736, Nov. 1982.

[40] T. G. Hodgkinson *et al.*, "In-phase and quadrature detection using 90° optical hybrid receiver: Experiments and design considerations," *IEE Proc. J. Optoelectron.*, vol. 135, pp. 260–267, Jun. 1988.
[41] M. L. Farwell, W. S. C. Chang, and D. R. Huber, "Increased linear dynamic range by low biasing the Mach-Zehnder modulator," *IEEE Photon. Technol. Lett.*, vol. 5, no. 7, pp. 779–782, Jul. 1993.
[42] P. Hariharan, "Two beam interference," in *Optical Interferometry*, 2nd ed. Amsterdam, The Netherlands: Elsevier, 2003, pp. 9–34.
[43] V. J. Urick, M. E. Godinez, P. S. Devgan, J. D. McKinney, and F. Bucholtz, "Analysis of an analog fiber-optic link employing a low-biased Mach-Zehnder modulator followed by an Erbium-doped fiber amplifier," *J. Lightw. Technol.*, vol. 27, no. 12, pp. 2013–2019, Jun. 2009.
[44] P. Hariharan, "Coherence," in *Optical Interferometry*, 2nd ed. Amsterdam, The Netherlands: Elsevier, 2003, pp. 35–58.

Ross T. Schermer (M'01) received the B.A. degree in physics from Gustavus Adolphus College, St. Peter, MN, USA, in 1999, and the M.S. and Ph.D. degrees in electrical engineering from the University of Minnesota, Minneapolis, MN, USA, in 2002 and 2004, respectively.

From 2004 to 2007, he was a Postdoctoral Research Associate with the U.S. Naval Research Laboratory, supported by a grant from the National Research Council. Since 2007, he has been a Research Physicist with the U.S. Naval Research Laboratory, Optical Sciences Division, Washington, DC, USA. He has authored more than 25 publications and holds five U.S. patents. His research interests include photonics for communications and sensing, guided-wave electro-optics, and optoelectronic materials.

Jason D. McKinney (M'03–SM'10) heads the Microwave Photonics Section, Optical Sciences Division, U.S. Naval Research Laboratory, Washington, DC, USA. His group focuses on optical sampling and processing of microwave signals, novel high-fidelity analog link architectures, and optical techniques for array processing for a number of applications. In 2006, he joined the Optical Sciences Division. As an Engineer in the Microwave Photonics Section, he demonstrated the first analog optical link to achieve a noise figure below 10 dB and linearization techniques for phase-modulated analog optical links. His work in applying electro-optic combs in microwave photonic systems has led to the highest dynamic range single-span photonic link demonstrated to date as well as novel subsampled link architectures and signal disambiguation techniques. He has authored or coauthored more than 80 refereed journal and conference papers, holds five U.S. patents, and is coauthor of the text *Fundamentals of Microwave Photonics*.